

Dissociative electron attachment and vibrational excitation of CF₃Cl: Effect of two vibrational modes revisited

Michal Tarana,^{1,2,*} Karel Houfek,³ Jiří Horáček,³ and Ilya I. Fabrikant^{1,4,†}

¹*Department of Physics & Astronomy,
University of Nebraska, Lincoln, NE 68588, USA*

²*JILA, University of Colorado and NIST,
Boulder, Colorado 80309-0440, USA*

³*Institute of Theoretical Physics, Faculty of Mathematics and Physics,
Charles University in Prague, V Holešovičkách 2, Prague, Czech Republic*

⁴*Department of Physics and Astronomy, The Open University,
Walton Hall, Milton Keynes MK7 6AA, UK*

Abstract

We present a study of dissociative electron attachment and vibrational excitation processes in electron collisions with the CF₃Cl molecule. The calculations are based on the two-dimensional nuclear dynamics including the C-Cl symmetric stretch coordinate and the CF₃ symmetric deformation (umbrella) coordinate. The complex potential energy surfaces are calculated using the *ab initio* R-matrix method. The results for dissociative attachment and vibrational excitation of the umbrella mode agree quite well with experiment while the cross section for excitation of the C-Cl symmetric stretch vibrations is about a factor of three low as compared to experimental data.

* michal.tarana@jila.colorado.edu

† iif@unlserve.unl.edu

I. INTRODUCTION

Dissociative electron attachment (DEA) to polyatomic molecules typically involves multidimensional nuclear dynamics. However, because of big computational work necessary to obtain multidimensional complex (*i.e.*, including both real and imaginary parts) energy surfaces, most of theoretical DEA calculations were performed in one-dimensional approximation. In these calculations it is usually assumed that the DEA process involves one reaction (dissociating) coordinate, roughly corresponding to one of the normal modes of the target molecule. This approximation is sometimes too crude, and sometimes completely unjustified. Therefore, a lot of effort was devoted recently to calculations of multidimensional DEA dynamics [1–6]. These calculations address two important problems in the physics of DEA processes. First, we want to know which dissociation channels are the most important and what is the energy range where a particular bond breaking can occur. This information is especially important for chemical control. Second, we want to know the importance of different vibrational modes in a particular DEA process and the final-state vibrational energy distribution in the fragments.

The most common method for studies of dynamics on multidimensional surfaces is the wave-packet propagation technique [7]. Recently, this approach was used to calculate the DEA cross sections for several polyatomic molecules, e.g. for CO₂ [8] or H₂O [9], employing the multi-configuration time-dependent hartree (MCTDH) method [10, 11]. An alternative is to develop classical and semiclassical methods for treatment of nuclear dynamics. We recently reformulated [1] the quantum method for DEA in terms of the time-independent Schrödinger equation and connected this treatment with the classical approximation. The method was applied to the process



Here ν_2 and ν_3 stand for the symmetric deformation vibrations (so-called “umbrella” mode) and the symmetric stretch vibrations, ν'_2 represents the umbrella mode of the free CF₃ radical. The two-mode approximation for this process can be justified by existing experimental data [12] on vibrational excitation (VE) of this molecule. The two-dimensional potential energy surface (PES) was calculated *ab initio*. However, we used a model semiempirical width (the imaginary part of the complex PES). This led to some inconsistencies and instabilities in our calculations discussed below. In the present paper we employ the *ab initio*

42 molecular *R*-matrix method for calculation of the complex PES. This allows us to remove
 43 the deficiencies in our previous calculations and improve agreement with experimental data.
 44 We also calculate VE cross sections for the C–Cl symmetric stretch and the umbrella mode.
 45 The rest of the paper is organized as follows. In Sec. II we discuss construction of the
 46 complex PES from the *ab initio* calculations and the our theoretical approach to treatment
 47 of nuclear motion. In Sec. III we discuss details of our *R*-matrix scattering calculations in
 48 the fixed-nuclei approximation. In Sec. IV we present our results for DEA and VE.

49 II. THEORETICAL APPROACH

50 In our previous work [1] we constructed a two-dimensional local complex potential (LCP)
 51 model for DEA and resonant VE of CF₃Cl. The model takes into account the C–Cl stretching
 52 vibrational mode and umbrella vibrational mode of the CF₃ radical. The LCP model [1] was
 53 based on a complex PES constructed from the one-dimensional potential curves using an
 54 arbitrary extension in the coordinate corresponding to the umbrella vibrations of the CF₃
 55 fragment. In addition, the real part of the complex potential curve for the temporal anionic
 56 complex was obtained using the *ab initio* methods for bound-states calculations, while the
 57 imaginary part was obtained by fitting [13] the experimental results of Mann and Linder
 58 [12]. Cross sections of the DEA calculated using the two-dimensional model are factor of
 59 three higher than experimental values and one-dimensional non-local calculations [13]. This
 60 discrepancy was attributed to the inconsistencies between the real and imaginary part of
 61 the complex PES used in the model [1]. It is the aim of this work to construct a two-
 62 dimensional model of the nuclear dynamics along the same lines as in [1], however using
 63 a more consistent complex PES. We performed molecular *ab initio* *R*-matrix scattering
 64 calculations in the fixed-nuclei approximation for a set of nuclear geometries including both
 65 degrees of freedom corresponding to the C–Cl distance R and F–C–Cl angle ϑ . We fitted
 66 the eigenphases obtained from these *R*-matrix calculations at energies close to the resonance
 67 position to the Breit-Wigner formula with an energy-dependent background [14] and using
 68 the resonance position and width we constructed the complex PES. This approach is free of
 69 any presumption on the dependence of the complex PES on the F–C–Cl angle and removes
 70 the need for any arbitrary extension in this coordinate used in [1]. In addition, the fixed-
 71 nuclei resonance width is calculated at the same level of the theory as the position.

72 The *ab initio* molecular R -matrix method is well known and widely used for fixed-nuclei
73 calculations of electron collisions with small and medium-sized molecules. We refer the
74 reader to a recent review article by Tennyson [15] and to references therein for description
75 of the method and its technical implementation.

76 The eigenphase sums calculated using the R -matrix method for a set of nuclear geome-
77 tries were fitted using the Breit-Wigner formula taking into account the dominant dipole
78 component of the potential in the outer region. The Breit-Wigner formula is equivalent
79 to the one-pole approximation to the R -matrix [14]. This approximation is based on the
80 assumption that at the energies close enough to the resonance position the R -matrix can be
81 well approximated by the following expression:

$$R(E) = R_0 + \frac{\gamma_\lambda^2}{E_\lambda - E}, \quad (2)$$

82 where R_0 is the background R -matrix including all the terms due to remaining poles of the
83 R -matrix, E_λ is position of the pole closest to the resonance, γ_λ is corresponding amplitude
84 and E is the scattering energy. To obtain the Breit-Wigner formula from Eq. (2), we
85 assume that the term R_0 is a slowly varying function of energy as it is sum over all the other
86 R -matrix poles. The eigenphase sum δ may then be expressed [14] as

$$\delta(E) = \tan^{-1} \left(\frac{\frac{1}{3}\Gamma_\lambda}{E_\lambda + \Delta_\lambda - E} \right) - \phi(E), \quad (3)$$

87 where Γ_λ is the resonance width and Δ_λ is the level shift (amount by which the resonance
88 energy is shifted from the pole E_λ). The first term of Eq. (3) describes the resonance contri-
89 bution and the second ($\phi(E)$) the potential scattering contribution. The relations between
90 Γ_λ , Δ_λ , ϕ and general solutions of the Schrödinger equation on the R -matrix boundary are
91 given in Ref. [14]. In order to fit the width and the position of the resonance using this model
92 we first solve the Schrödinger equation with the dipole potential in the outer region. The
93 corresponding dipole moment for every nuclear geometry is obtained from the *ab initio* cal-
94 culation of target properties as a part of the fixed-nuclei scattering calculations. Having the
95 solutions on the R -matrix boundary we can establish the relation between the background
96 phase shift $\phi(E)$, width Γ_λ , level shift Δ_λ and quantities in Eq. (2). This allows us to fit
97 the model R -matrix amplitude γ_λ , pole E_λ and constant background R -matrix R_0 using the
98 non-linear least-squares technique to the *ab initio* eigenphase sum. These directly determine
99 the width Γ_λ and resonance energy $E_\lambda + \Delta_\lambda$. This fitting allows for a construction of the

complex PES $U(R, r) - i\Gamma(R, r)/2$ in the region where the anionic state is metastable. In the region where the resonance turns into a bound state, the corresponding bound state energy was calculated as well as the potential energy curve $V(\infty, r)$ of the free CF_3 fragment. The complex PES was constructed using cubic splines in two dimensions. In order to study the final-state interaction on the anionic surface during the DEA process, it was necessary to have the bound anionic PES also for large C–Cl internuclear separations, where the *ab initio* results are not available. It was constructed by the extrapolation of the *ab initio* results as described in [1] to satisfy the condition $U(R \rightarrow \infty, r) \rightarrow V(\infty, r)$. The bound part of the anionic potential energy surface was extrapolated to match the CF_3 fragment potential curve asymptotically, as discussed in [1].

The LCP calculations of the DEA and VE presented here were performed in a similar way as described in Ref. [1]. The basic equation of the LCP theory reads

$$[T_\rho + T_r + U(\rho, r) - i\Gamma(\rho, r)/2 - E]\chi_E(\rho, r) = V_{dk}(\rho, r)\zeta_i(\rho, r), \quad (4)$$

where ρ and r are the reaction coordinates introduced to decouple the two-dimensional operator of the nuclear kinetic energy [1]. $U(\rho, r) - i\Gamma(\rho, r)/2$ is the complex PES of the temporal anion, $V_{dk}(\rho, r) = \sqrt{\Gamma(\rho, r)/2\pi}$ is the amplitude for electron capture into the resonance state and $\zeta_i(\rho, r)$ is the vibrational wave function of the neutral molecule in the initial state. $T_\rho + T_r$ is the operator of nuclear kinetic energy corresponding to our two-dimensional model as discussed in [1]. In our previous work [1] the wave function $\chi_E(\rho, r)$ was expanded in the basis of vibrational states $\phi_\nu(r)$ of the CF_3 fragment in the harmonic approximation given by equation

$$[T_r + V^h(\infty, r) - \epsilon_\nu]\phi_\nu(r) = 0, \quad (5)$$

where ϵ_ν are the corresponding eigenenergies $\epsilon_\nu = D_e + \omega_2^f(\nu + 1/2)$, ω_2^f is the harmonic frequency of the CF_3 radical umbrella mode and $V^h(\infty, r)$ is the corresponding free CF_3 radical potential curve in the harmonic approximation with the minimum corresponding to the C–Cl bond dissociation energy. As it is explained in [1], projection of Eq. (4) on $\phi_\nu(r)$ then yields a set of coupled differential equations for channel wave functions of the variable ρ with coupling potential $U_{\nu\nu'}(\rho)$ given by the equation

$$U_{\nu\nu'}(\rho) = \int \phi_\nu(r) [U(\rho, r) - i\Gamma(\rho, r)/2 - V^h(\infty, r)] \phi_{\nu'}(r) dr. \quad (6)$$

126 One note should be made at this point regarding the asymptotic behavior of the coupling
 127 potential. The PES in [1] was extrapolated in such way that $U(R \rightarrow \infty, r) \rightarrow V(\infty, r)$.
 128 The extrapolation asymptotically matches the *ab initio* potential energy curve of the CF_3
 129 fragment, not its harmonic approximation. As a consequence, $\lim_{\rho \rightarrow \infty} U_{\nu\nu'}(\rho) \neq 0$, as can
 130 be seen in Eq. (6). Since the coupling of different vibrational channels of the CF_3 radical
 131 doesn't vanish for $\rho \rightarrow \infty$, population of different vibrational states of CF_3 produced by the
 132 DEA process does not converge well. This deficiency is corrected in the present work. The
 133 harmonic approximation for the potential energy curve $V^h(\infty, r)$ of the CF_3 radical is not
 134 used and the full *ab initio* potential curve $V(\infty, r)$ is employed in both Eq. (5) and Eq. (6).
 135 Therefore, in our present calculations we expand the wave function $\chi_E(\rho, r)$ in the basis set
 136 of eigenfunctions $\varphi_\nu(r)$ given by the equation

$$[T_r + V(\infty, r) - \varepsilon_\nu] \varphi_\nu(r) = 0, \quad (7)$$

137 where ε_ν are the vibrational energies of the CF_3 fragment without the harmonic approxima-
 138 tion. The corresponding coupling potential has the following form:

$$U_{\nu\nu'}(\rho) = \int \varphi_\nu(r) [U(\rho, r) - i\Gamma(\rho, r)/2 - V(\infty, r)] \varphi_{\nu'}(r) dr. \quad (8)$$

139 Therefore, in the present work the extrapolated PES is consistent with the asymptotic
 140 treatment of the CF_3 fragment that allows for convergence of the population of vibrational
 141 states of CF_3 produced by the DEA process.

142 In the present work we also use a different method to solve the system of coupled ra-
 143 dial equations. In Ref. [1] we used direct outward integration of the system of differential
 144 equations from the inner region and inward integration from the asymptotic region with
 145 subsequent matching of the solutions to satisfy the boundary conditions. The direct inte-
 146 gration has a limitation in number of channels included in the calculation. With increasing
 147 number of closed channels included, their exponentially increasing contribution starts to be
 148 more pronounced and the calculation becomes unstable.

149 Here we employ the multichannel version of the exterior complex scaling (ECS) method in
 150 the discrete variable representation (DVR) basis set [16], which is free of this problem. This
 151 method has previously been successfully used in the context of nonlocal resonance model
 152 for calculations of DEA and VE in case of diatomic molecules [17].

153 III. SCATTERING CALCULATIONS IN THE FIXED-NUCLEI APPROXIMA- 154 TION

155 In order to obtain the two-dimensional complex PES necessary to construct the LCP
156 model, we performed the R -matrix scattering calculations in the fixed nuclei approximation
157 for a set of nuclear geometries important for the DEA and VE. For every nuclear geometry we
158 calculated the eigenphase sum in the energy interval around the fixed-nuclei resonance and
159 fitted it to the Breit–Wigner formula with background as described above. The resonance
160 position and width as a function of the nuclear coordinates represent the complex PES
161 used in the local complex approximation. In the region where the CF_3Cl^- anion is stable
162 against autodetachment and the potential becomes real, the surface is represented by the
163 bound-state energies calculated using the R -matrix approach.

164 As it was discussed previously [1], in our calculations the PES V and U for the neutral
165 molecule and for the anion are represented using two coordinates: C-Cl internuclear separa-
166 tion R and the distance between the C atom and the plane formed by the fluorine atoms
167 $r = -R_{CF} \cos \vartheta$, where ϑ is the F-C-Cl angle and R_{CF} is the F-C bond length. Since we
168 do not include the C-F stretching mode into our considerations, R_{CF} is fixed and set to
169 the value 1.342 Å corresponding to the equilibrium geometry of the neutral CF_3Cl . The
170 fixed-nuclei R -matrix calculations were performed for a two-dimensional region of nuclear
171 coordinates with R from $3 a_0$ to $12 a_0$ and with ϑ from 55° to 90° . In the present work we
172 consider excitation of the low vibrational states of the CF_3 fragment only, therefore we don’t
173 take into account any effects caused by the flipping of the radical ($\vartheta > 90^\circ$).

174 Calculations were performed using Gaussian type orbitals (GTOs) and the UK polyatomic
175 R -matrix code [15]. The highest symmetry available in the polyatomic code is C_s which is
176 an abelian subgroup of the true C_{3v} symmetry of CF_3Cl .

177 A. Target representation

178 The CF_3Cl was represented using Hartree–Fock (HF) molecular orbitals (MOs). In order
179 to construct a target model sufficient for the purpose of the dynamical calculations, we
180 performed several tests with different target models to select the best compromise between
181 the quality of the target representation and the computational tractability of the $(N + 1)$ -

182 particle problem.

183 The CF_3Cl target states were represented using a complete active space (CAS) config-
 184 uration interaction (CI) wave function. The CF_3Cl molecule contains 50 electrons. Only
 185 18 of them belong to the inner shells, 32 remaining electrons form the valence shells and
 186 in principle can contribute to the chemical bonds. This complicates the construction of the
 187 target CI model in several aspects. Enough valence electrons should be included in the CI
 188 active space to treat the electron correlation properly. In addition, it is necessary to treat
 189 the target symmetrically and to ensure that all elements of the degenerated pairs of MOs
 190 are included in the CAS. On the other hand, inclusion of each orbital occupied in the HF
 191 ground state leads to a rapid increase in dimension of the target and anionic CI Hamiltoni-
 192 ans. In addition, it is the aim of our fixed-nuclei calculations to study the dependence of the
 193 resonance on the nuclear geometry. This raises further the limitations on the $N + 1$ -particle
 194 CI calculation as we need to repeat it many times.

195 The first CAS CI target model considered in our calculations includes eight active elec-
 196 trons which occupy four orbitals in the HF ground state determinant with the highest orbital
 197 energies. We allow these electrons to occupy five lowest virtual orbitals (VOs). Using the
 198 notation of the C_s point group, this CAS model can be expressed as follows:

$$(1a' \dots 15a')^{30}(1a'' \dots 6a'')^{12}(16a' \dots 21a', 7a'' \dots 9a'')^8 \quad (9)$$

199 OR

$$(1a' \dots 15a')^{30}(1a'' \dots 6a'')^{12}(16a' \dots 20a', 7a'' \dots 10a'')^8, \quad (10)$$

200 as the ordering of VOs changes with nuclear geometry. Using the notation of the C_{3v} point
 201 group, the active electrons are taken from the following set of HF orbitals: $(1a_2, 10a_1, 7e)$.
 202 The degenerated e -orbitals in this set are well localized on the chlorine atom, the $10a_1$ -
 203 orbital is spread along the C–Cl bond and the $1a_2$ orbital contributes to the C–F bonds.
 204 The calculations were performed using the 6-311G* GTO basis set [18, 19].

205 Representation of the target in the subsequent scattering calculation can be qualified by
 206 comparison of several properties calculated using our model with the previously published
 207 results. To check our target representation, we calculated the vertical excitation energy
 208 (as the excited target states are used in the scattering calculations), dipole moment of the
 209 target ground state (as it represents the major contribution to the interaction with the
 210 projectile in the outer region) and static dipole polarizability which allows us to estimate

the representation of the polarization effects in the scattering calculation. Comparison of values calculated using our models (at equilibrium nuclear geometry) with the previously published data is shown in Table I. As it can be seen there, this target model (denoted

TABLE I. Target properties calculated using different CAS CI models at equilibrium nuclear geometry and their comparison with the previously published results.

	Model 1	Model 2	Bibliographical data
GTO basis	6-311G*	cc-pVDZ	
# of active electrons / # of VOs	8/5	4/11	
Ground state energy (a.u.)	-795.787343	-795.627044	
Vertical excitation energy 1E (eV)	9.545	9.057	7.7 ± 0.1 [20, 21]
Vertical excitation energy 3E (eV)	8.476	7.897	
Dipole moment (a.u.)	0.378	0.410	0.197 [22]
Static dipole polarizability (a.u.)	1.32	0.158	38.6 [22]

214
215

TABLE II. Vibrational frequencies calculated using different CAS CI models and their comparison with the previously published results.

	Model 1	Model 2	Bibliographical data
ω_2 (cm^{-1})	854.42	956.48	775.12 [23]
ω_3 (cm^{-1})	433.08	534.13	463.33 [23]
CF ₃ fragment (ω_2) (cm^{-1})	755.53	745	701 [24]

216
217

as Model 1 there and elsewhere in the text) gives a reasonably good representation of the ground state dipole moment, as it is relatively small, although our calculation gives us a larger value than found in the experiment. The vertical excitation energy calculated here is almost 2 eV higher than the experimental value [21]. It suggests that the representation of the target excited states is limited. According to our knowledge, there is no experimental or advanced theoretical calculation of the lowest excited state 3E available. Our target model gives its energy 8.453 eV above the ground state. In our scattering calculations, we are

225 interested in scattering energies below 4 eV, where all the electronically excited channels are
226 closed. We expect (and our test calculations described below suggest it) that inclusion of
227 the low excited target states in the close-coupling (CC) expansion leads to a small correction
228 of the resonance position and width only.

229 In order to estimate how well are the polarization effects represented in our scattering
230 calculations, we evaluated the static dipole polarizability of the target ground state. We
231 used the sum-over-states formula with the set of target states included in the scattering
232 calculation. We found that the lowest six target states represent a considerable contribution.
233 Adding more target states did not increase the value. As can be seen in Table I, our
234 calculated value is considerably smaller than the experimental results. Since the higher
235 excited states do not have significant contribution to the polarizability, this discrepancy
236 can be possibly attributed to low number of active electrons and orbitals used in our target
237 model. Good representation of the polarizability would require presence of more diffuse MOs
238 which are too high in energy to be included in the present target calculations. However, the
239 previously published one-dimensional calculations of the nuclear dynamics for CF_3Cl [13]
240 show that the polarization effects have a minor effect on the results of the LCP calculations.

241 Target properties discussed above are all calculated at the equilibrium nuclear geometry.
242 However, for our calculations of the nuclear dynamics it is important to know how well can
243 our target model reproduce the harmonic vibrational frequencies of the neutral molecule.
244 Comparison of our calculated values with the previously published result is showed in Ta-
245 ble II. Our target model 1 gives the values with 10% accuracy when compared with the
246 experimental results. This small difference can be possibly attributed to the neglect of other
247 vibrational degrees of freedom in our model.

248 We can conclude that our CAS CI model 1 represents the neutral target sufficiently
249 enough to be used in our *ab initio* R -matrix calculation. R -matrix calculations performed
250 at the equilibrium nuclear geometry can be used to obtain the vertical attachment energy.
251 Correct value of this quantity is essential for our calculations of the resonant nuclear dy-
252 namics. However, the CAS CI model 1 of the target leads to the value which is 1.3 eV
253 above the experimental value determined by Aflatooni and Burrow [25]. Additional testing
254 calculations show that it is due to insufficient treatment of the electron correlation in the
255 CC expansion of the $N + 1$ -electron wave function. Since further increase of the number of
256 active electrons or VOs included in the target model leads to intractable diagonalization of

the $N + 1$ -electron Hamiltonian, we decided to model the electron correlation by modification of the primary GTO basis set, where we modified the gaussian exponent corresponding to the p-orbital of the chlorine atom in order to get the energy of the lowest unoccupied molecular orbital (LUMO) closer to the experimental value of the vertical attachment energy. We expect that this modified LUMO helps to represent the discrete component of the resonant wave function of the temporal anionic complex better than the linear combination of VOs obtained in model 1. This idea is similar to the method developed in Ref. [26] used to calculate the position and width of the resonance. The modified HF orbitals were calculated using the cc-pVDZ GTO basis set [27]. To approach the correct value of vertical attachment energy we changed the exponent of the uncontracted p-orbital of chlorine from 0.162 to 0.094. In addition to this modification of the exponent, we also restricted the CAS CI model to four active electrons from the highest occupied molecular orbital (HOMO) and HOMO-1 and allowed their excitations into 11 lowest VOs. Using the notation of the C_s point group, this CAS model can be expressed as follows:

$$(1a' \dots 16a')^{32}(1a'' \dots 7a'')^{14}(17a' \dots 25a', 8a'' \dots 11a'')^4 \quad (11)$$

OR

$$(1a' \dots 16a')^{32}(1a'' \dots 7a'')^{14}(17a' \dots 24a', 8a'' \dots 12a'')^4, \quad (12)$$

as the ordering of VOs changes with nuclear geometry. Therefore, in this model we extend the space of VOs and reduce the number of active electrons as compared with model 1. Properties of the target calculated at the equilibrium nuclear geometry are summarized in Table I (we refer to this model as to Model 2 in the table and elsewhere in the text below). It shows that although the ground state energy is higher than the value calculated using model 1, the vertical excitation energy into the 1E state is lower and closer to the published reference value. This CAS model of the target also gives lower vertical excitation energy to the 3E state than model 1. Table I also shows that this modified model gives larger value of the dipole moment than model 1, however its value is still low enough to not to introduce a significant error in the position and width of the resonance. We also calculated the static dipole polarizability at equilibrium nuclear geometry using this model and found that its value is significantly smaller than that given by experiment. This can be due to the limited representation of the polarization effects by the primary GTO basis set. Although both our CAS models of the target have their limitations, model 2 using the modified primary GTO

286 basis represents correctly the vertical attachment energy, the quantity which is essential for
 287 the DEA calculations.

288 In addition to the CAS model of the target we need a representation of the CF_3 fragment
 289 in our LCP calculations in order to extrapolate the potential energy surfaces properly. In
 290 order to keep the model of the fragment consistent with the target model 2, we treated the
 291 CF_3 radical at the SCF level as all the excitations of the active electrons in model 2 of the
 292 CF_3Cl target describe the C–Cl chemical bond. Therefore, any CI excitation model of the
 293 fragment would introduce a correlation which is not explicitly included in the target model.
 294 In order to check the quality of this representation we calculated the harmonic frequency
 295 of the umbrella mode. Its comparison with previously published value is given in Table II.
 296 It shows that our calculated harmonic frequency is slightly higher than the experimental
 297 value, but they are in a good agreement to confirm that our model is a suitable choice for
 298 representation of the CF_3 radical.

299 B. Scattering model

300 The R -matrix calculations were performed using a sphere with radius $r_\Omega=15\text{ a}_0$. Cor-
 301 responding continuum basis set was represented by single-center uncontracted GTOs with
 302 exponents optimized by the program GTOBAS [28]. Partial waves up to $l = 3$ (9s, 7p, 7d,
 303 7f) were used. The deletion threshold in the orthogonalization procedure for the continuum
 304 orbitals [15] was set to $\delta_{\text{thr}} = 9 \times 10^{-6}$. This value was found by performing calculations
 305 in the static exchange approximation. It gives a stable representation of the scattering
 306 continuum and does not show any problems related to linear dependence of the continuum
 307 orbitals.

308 In order to obtain the position and width of the fixed-nuclei resonance as a function of the
 309 nuclear geometry we performed a scattering calculation of the eigenphases and fitted them
 310 using the Breit-Wigner formula with the energy dependent background [14] as discussed
 311 above. We tested both CAS CI models of the neutral target discussed above. First, the
 312 lowest 16 CI target states calculated using Model 1 were used in the CC expansion and
 313 the R -matrix calculation at equilibrium nuclear geometry. This calculation gives converged
 314 results with respect to the number of target states included.

315 The corresponding cross section for elastic 2A_1 scattering is presented in Fig. 1 where we

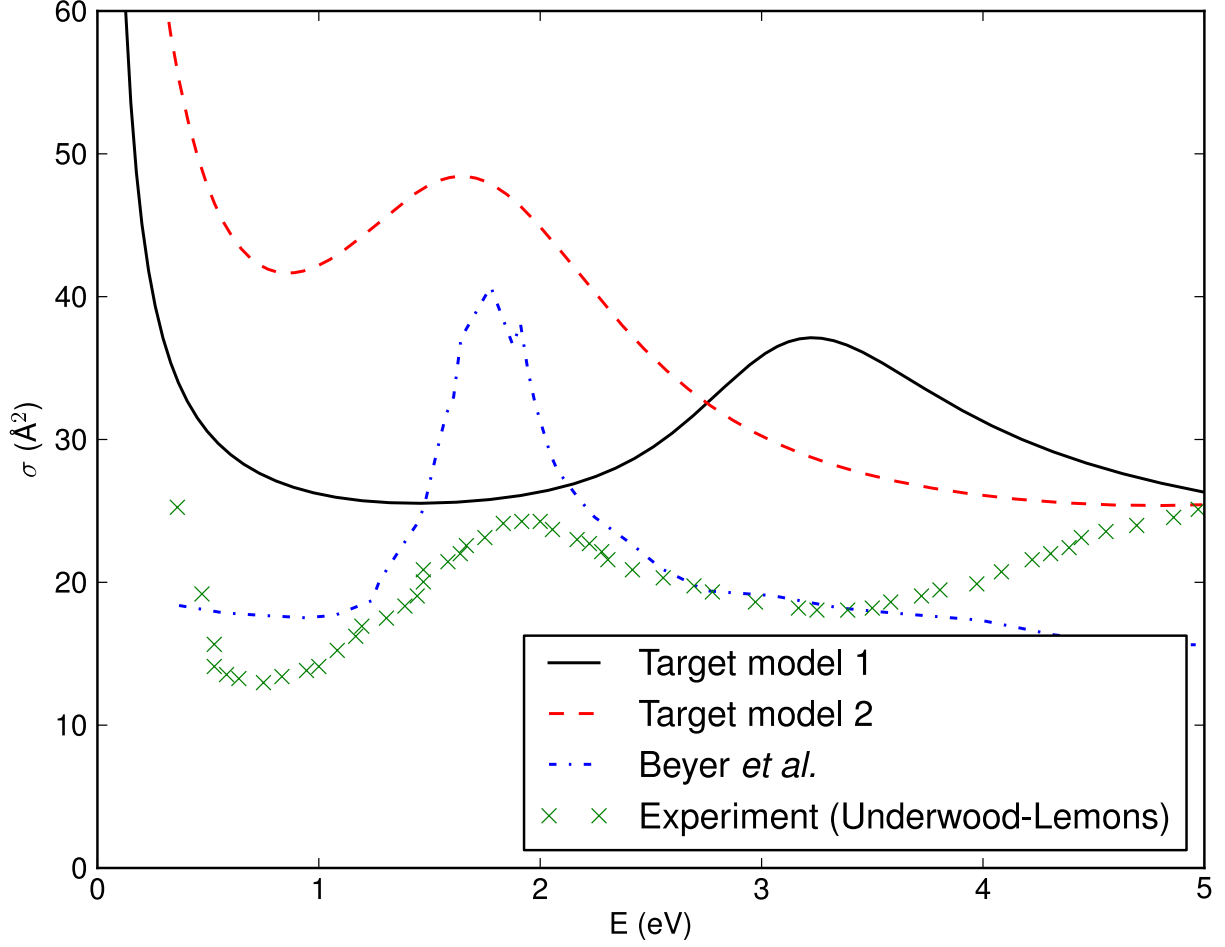


FIG. 1. Cross section for the elastic electron scattering off CF_3Cl (2A_1 symmetry) calculated in the fixed-nuclei approximation at equilibrium nuclear geometry. Calculations employing target model 1 is compared with results calculated using model 2, with experimental results [30] and with other R -matrix calculation [29].

also compare it with calculations of Beyer *et al.* [29]. This curve (designated as Target model 1) shows the peak at energy around 3.3 eV that is significantly above the experimental value due to experimental work by Underwood-Lemons *et al.* [30] and the theoretical calculation of Beyer *et al.* [29]. Since a further increase of the number of target states included in the CC expansion did not lead to any considerable shift of the peak towards lower energies, it suggests that this artificially high position of the resonance is not due to incorrect representation of the polarization effects [31], but rather due to an incompleteness of the target model. Therefore, we performed another set of scattering calculations using target CI model 2 described above. Since this model was constructed to reproduce the correct

vertical attachment energy, it also gives the correct position of the resonance peak in the R -matrix calculation carried at the equilibrium nuclear geometry (as plotted in Fig. 1). The rapid increase of the cross section at lower energies is due to the long-range dipole potential included in the outer region. For a molecule with a nonzero permanent dipole moment and fixed orientation the elastic cross section diverges at zero energy [32, 33], the feature which is observed in our cross section, but not in the calculation of Beyer *et al.* [29], apparently because the dipole effects were not included completely there. On the other hand, since our dipole moment at the equilibrium internuclear separation is too big (see Table I), it is evident that our elastic cross sections are strongly overestimated at low energies.

There were 12 target states included in our CC expansion (three lowest in singlet and triplet state of A' and A'' symmetries). The R -matrix was propagated in the dipole potential given by the target CAS CI model (as discussed above) and in the potential given by the dipole and quadrupole coupling of different scattering channels [15]. On the other hand, the R -matrix calculation of Beyer *et al.* [29] was performed at the level of static exchange with polarization which treats the electron correlation in a different way than our CAS CI model. This can be a partial reason of the quantitative difference between the two calculations at higher energies.

Fig. 1 also presents the experimental measurements of the total elastic cross sections by Underwood-Lemons *et al.* [30]. However, the problem with this and two other [12, 34] measurements for CF_3Cl is that it is not quite clear what is measured there. The total elastic cross section for a polar symmetric top is divergent even if rotations are included [35]. Only the inversion splitting, which is extremely small for CF_3Cl , makes the elastic cross section finite [36]. This means that the scattering amplitude at small scattering angle θ behaves like $1/\theta$, and only at an extremely small angle θ_{inv} it becomes finite. In the experiment of Underwood-Lemons *et al.* [30] the elastic cross section is determined from the transmitted current under the assumption that transmitted electrons are not scattered, therefore what is measured in fact is the cross section integrated from a small angle θ_{min} to 180° , where θ_{min} is determined by the geometry of the experimental apparatus, and θ_{min} is, most likely, significantly greater than θ_{inv} . In the experiment of Mann and Linder [12] the total cross section is obtained by extrapolating the measured differential cross section to $\theta = 0$. This procedure also gives an underestimated total cross section since the actual differential cross section behaves as $1/\theta^2$ at small angles, if $\theta > \theta_{inv}$. We think, therefore

that comparison between the theory and the experiment for the total (integrated) cross section is meaningless unless the angle θ_{\min} can be found from the experimental geometry. The purpose of plotting the experimental cross section in Fig. 1 is to demonstrate that our calculated resonance contribution is consistent with experimental results.

At larger C–Cl separations, where the resonance turns into a bound state, the corresponding anionic bound state energies were calculated by diagonalizing the $N + 1$ electron Hamiltonian constructed using the same target and scattering CAS CI model as was used for calculation of the resonance, just the integrals involving continuum GTOs were not restricted to the inner region of the sphere [15]. This allows a good representation of the diffuse character of the anionic bound state with energy close to the autodetachment limit.

The position and width of the fixed-nuclei resonance as a function of the nuclear geometry were obtained by fitting the eigenphases at energies close to the resonance to the Breit-Wigner formula with energy-dependent background performed at each nuclear geometry of our interest. The energy dependence of the background is predominately determined by the dipole moment of the neutral target. The corresponding value was obtained from the calculation of the target properties for every nuclear geometry and used as a parameter in the fitting procedure for this geometry. Fitting of the eigenphases calculated at equilibrium geometry using target model 2 gives a resonance position 1.954 eV, which is in a good correspondence with experimental value 1.83 eV due to Aflatooni and Burrow [25].

IV. CALCULATIONS OF THE NUCLEAR DYNAMICS

A. Dissociative electron attachment

The total DEA cross section calculated using our two-dimensional LCP approach is plotted in Fig. 2. This graph shows its comparison with previously published one-dimensional non-local calculations [13]. Our previously published two-dimensional LCP calculations [1] give significantly larger magnitude of the total DEA cross section than experimental works [25, 37] and one-dimensional non-local semiempirical calculation [13]. This problem was attributed to incorrect dependence of the width function (which was arbitrarily extended to two dimensions) on the coordinate r . As can be seen in Fig. 2, results of our present two-dimensional LCP calculations using the complex PES constructed from the

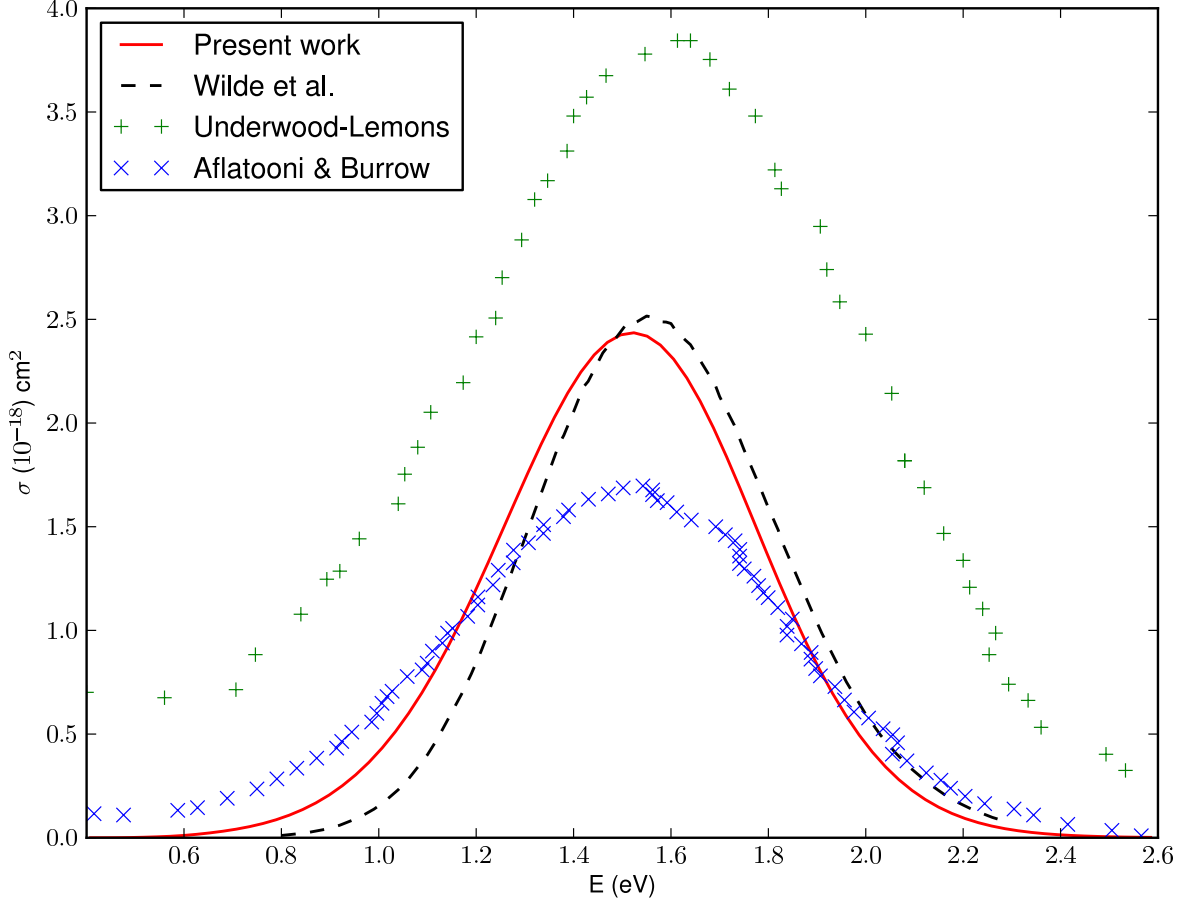


FIG. 2. Total DEA cross section calculated using the model discussed in the present work is compared with experimental results of Underwood-Lemons *et al.* [37], Aflatooni and Burrow [25] and with previously published one-dimensional non-local calculations due to Wilde *et al.* [13].

388 *R*-matrix results are in very good agreement with the non-local calculations as well as with
 389 experimental results due to Aflatooni and Burrow [25]. Although our total cross section is
 390 smaller than the experimental results of Underwood-Lemons *et al.* [37], it is closer to the
 391 measurements of Aflatooni and Burrow [25], and the position of the peak is in very good
 392 correspondence with this experimental work. All this suggests that the two-dimensional
 393 PES constructed from the results of the *R*-matrix calculations has more correct dependence
 394 on both reaction coordinates than the previously published model [1]. It results in a correct
 395 shift of the peak in the total DEA cross section with respect to the VAE as well as in the
 396 correct magnitude of the cross section. One additional note regarding the complex PES
 398 should be made here. The DEA cross section is related to the position of the crossing seam
 399 between the neutral and anionic PES. Its shape and position with respect to the minimum

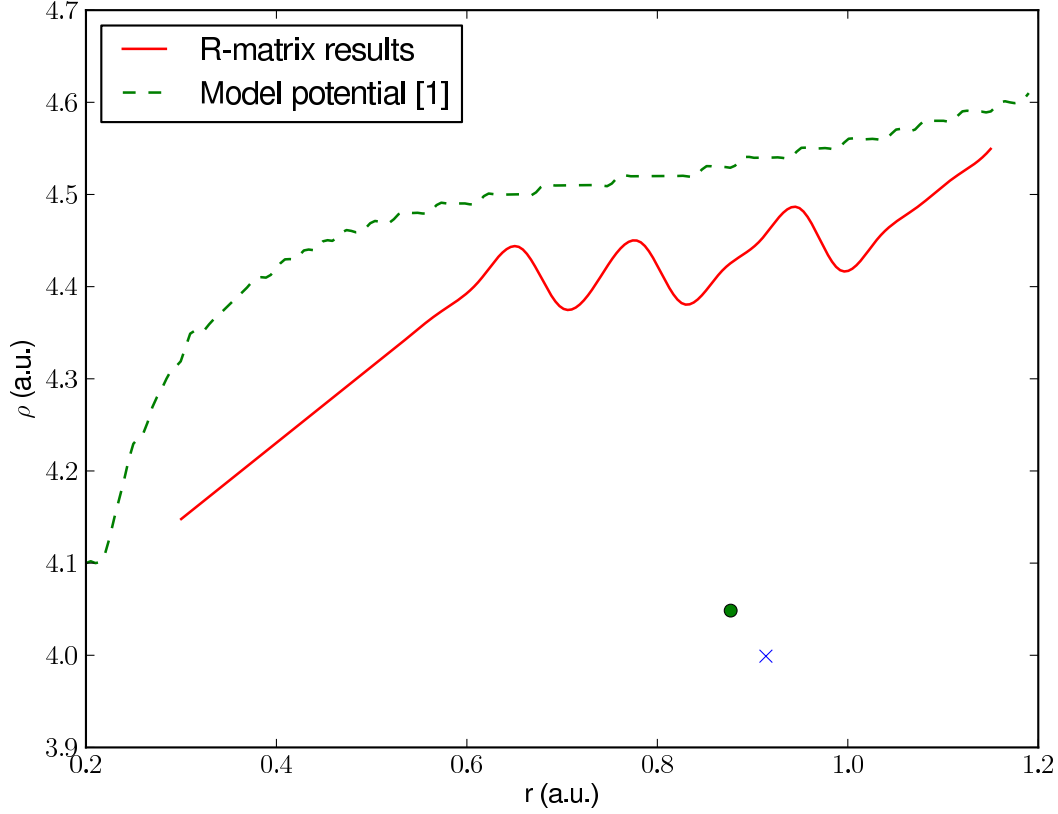


FIG. 3. The crossing seam between the neutral and anionic two-dimensional PES obtained from the present *R*-matrix calculations and its comparison with model potential used in [1]. The cross (circle) denotes the equilibrium geometry of the neutral PES obtained in the present work (used in [1]).

of the neutral PES determine where the anionic system becomes stable. Subsequently, it has an influence on the survival probability. The crossing seams obtained from the present *R*-matrix calculations and from the model potential [1] are compared in Fig. 3. The relative position of the crossing seam is similar in both models. This supports our argument that the difference in magnitude of the DEA cross section between our present model and the results published in [1] is mainly due to the different width function $\Gamma(\rho, r)$, rather than due to the substantial difference in the crossing seam between these two models. The oscillatory structure in the crossing seam obtained from the present *R*-matrix calculations is mainly an artifact of too low density of the grid of nuclear geometries used to calculate the PES.

409 In addition, the fact that the complex energies in the region, where the anion is metastable
 410 are obtained in different way than the eneries of the bound anion, also raises the numerical
 411 issues with exact determination of the crossing seam and partially also contibutes to the
 412 oscillatory structure present in Fig. 3.

413 Comparisons of local two-dimensional and one-dimensional results with nonlocal one-
 414 dimensional results are given in Refs. [1, 38]. The agreement between the local and non-
 415 local results is very good because the resonance occurs at a relatively large energy, and the
 416 long-range interaction plays a minor role.

417 Fig. 4 shows the distribution of different final vibrational states of the CF_3 fragment
 418 calculated using the complex PES constructed from the R -matrix results. In Fig. 5 we show
 419 the distribution calculated using the PES obtained in Ref. [1] but corrected in such a way
 420 that PES in the intermediate region smoothly turns into the PES in the asymptotic region
 421 avoiding the mismatch discussed in Sec. II. Both graphs show that the low vibrationally
 422 excited states of the CF_3 fragment will be more populated than the ground state and in
 423 both figures the positions of the peaks rise with increasing quantum number ν . However,
 424 each calculation predicts highest population for a different excited state. While our complex
 425 PES constructed from the R -matrix results gives the highest peak for $\nu = 1$, the PES
 426 described in [1] leads to the highest peak for vibrational state $\nu = 3$, as can be seen in
 427 Fig. 5. Total DEA cross section is mainly determined by the complex PES in the region
 428 where the anionic system is not bound and does not strongly depend on the behavior of
 429 the PES in the region where the negative ion is stable. On the other hand, the distribution
 430 of vibrational states of the fragment is strongly influenced by the final-state interaction in
 431 the region where the anion is stable. In both calculations shown in Fig. 4 and Fig. 5, this
 432 region of the PES was partially modeled (as discussed above and in [1]) to achieve correct
 433 asymptotic behavior of the potential. Although our PES constructed from the R -matrix
 434 results is free of several limitations of the surface described in [1], the extrapolation of the
 435 bound-state anionic surface in both cases makes it difficult to decide, how quantitatively
 436 reliable this distribution is in both calculations.

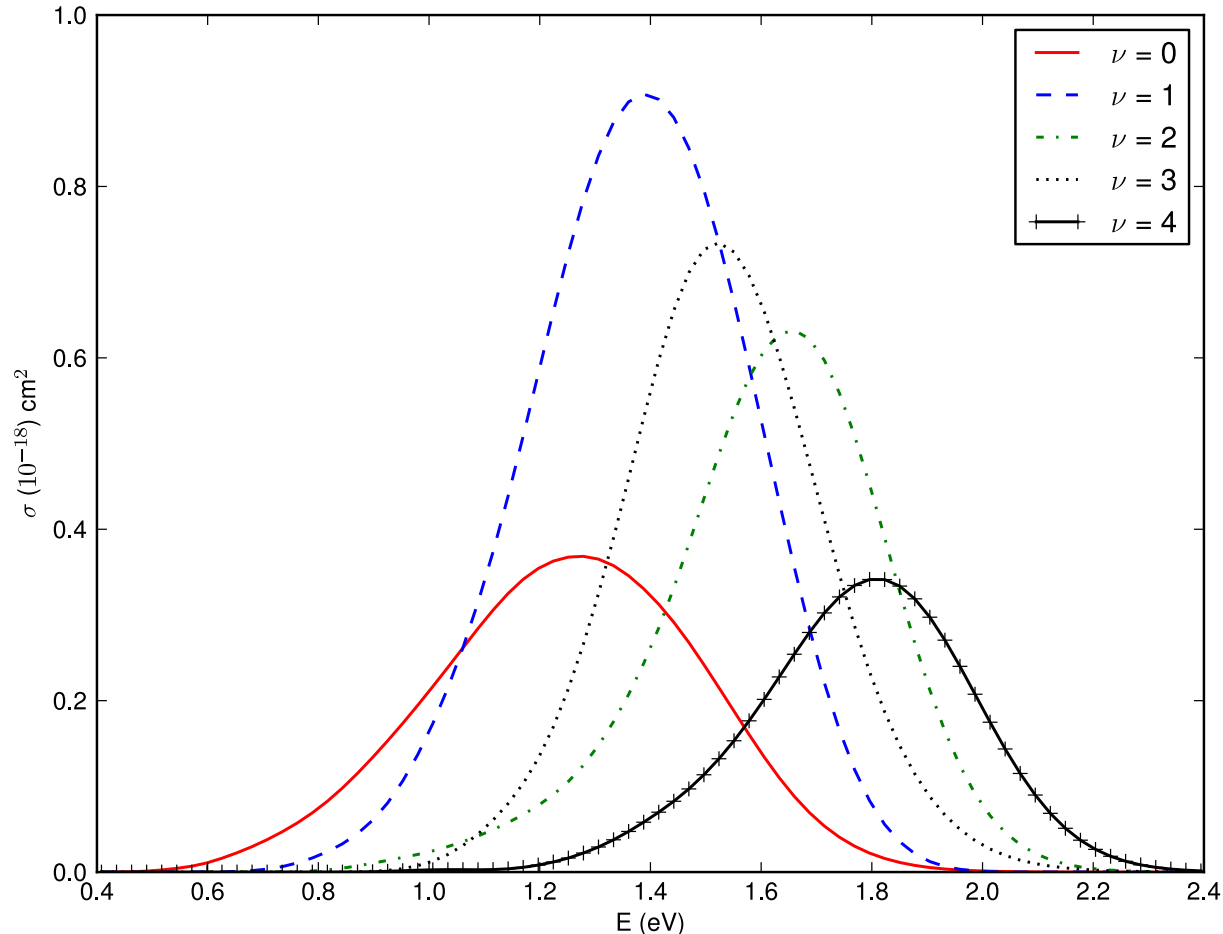


FIG. 4. DEA cross sections for different final vibrational states of the fragment CF_3 calculated using the complex PES constructed from our R -matrix results.

B. Vibrational excitation

Results of the resonant VE calculations using the PES based on the R -matrix results are plotted in Fig. 6. This figure shows the cross section for VE of the target from the ground state to the lowest excited state of the C–Cl stretching mode (denoted as $(0, 1)$ in the figure) and the lowest excited state of the C–F deformation mode (denoted as $(1, 0)$ in the figure). These graphs show a very good agreement with our previous calculations [1] for both vibrational modes. However, our calculations agree with experimental results by Mann and Linder [12] for the umbrella mode, while both our models lead to approximately three times smaller magnitude of the cross section for the C–Cl stretching mode excitation than that measured by Mann and Linder [12].

The previously published one-dimensional non-local calculation of VE [13] takes into

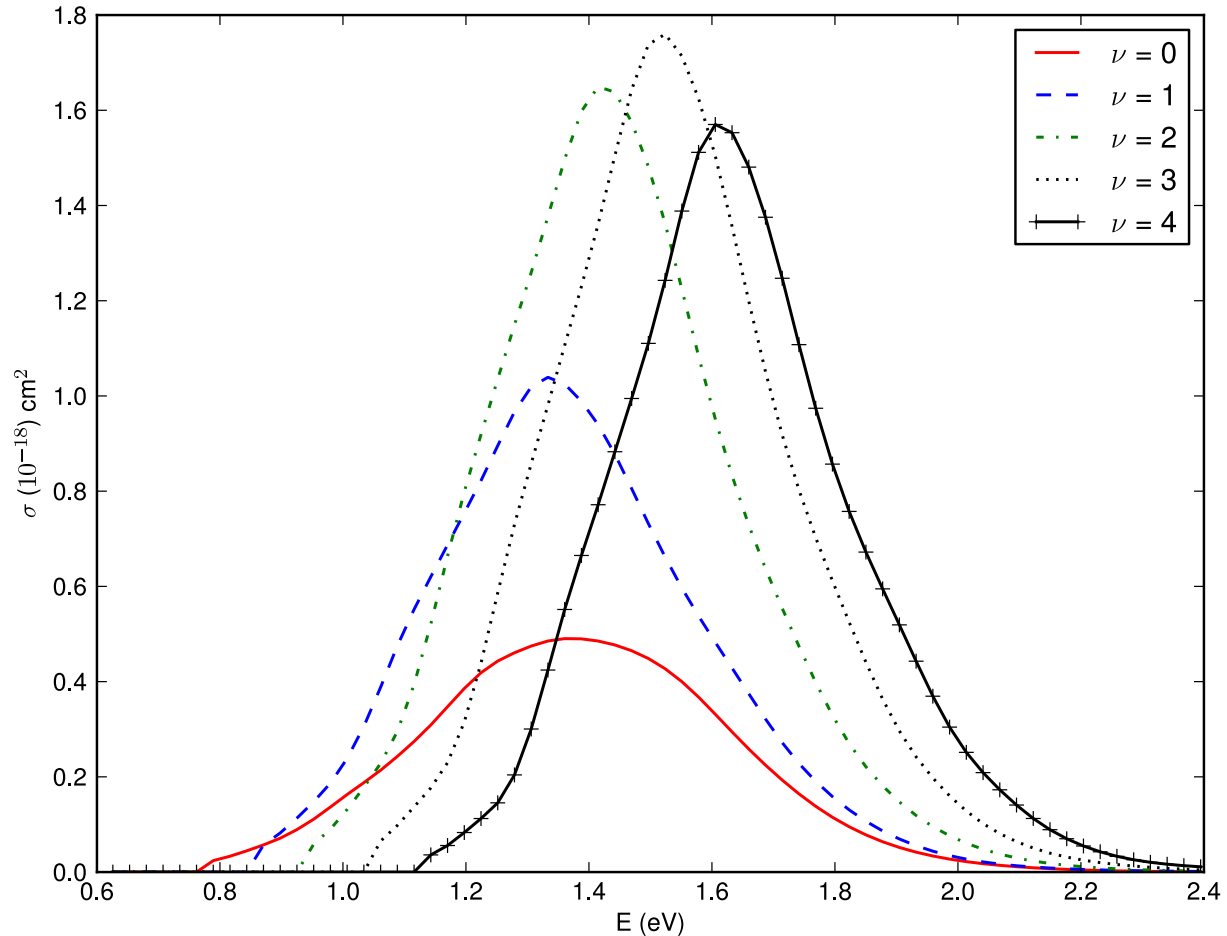


FIG. 5. DEA cross sections for different final vibrational states of the fragment CF_3 calculated using the model complex PES published previously [1] after the correction of the asymptotic behavior of channel potentials.

account the C-Cl stretching vibrational mode only and the width function $\Gamma(R)$ was adjusted to give cross sections corresponding to experimental results for this stretching vibrational modes excitation due to Mann and Linder [12]. The low values of the present cross sections can be partially explained by introduction of additional channels of vibrational excitation in our two-dimensional calculations and lower flux towards the channel (0, 1).

Although Fig. 6 shows that the model constructed using the R -matrix results leads to VE cross sections very similar to those calculated in Ref. [1], Fig. 7 shows that these two models predict different results for higher final vibrational states. To our best knowledge, there are no experimental data for VE to these states to compare with our cross sections. The fact that the differences between our two models become more significant with increasing

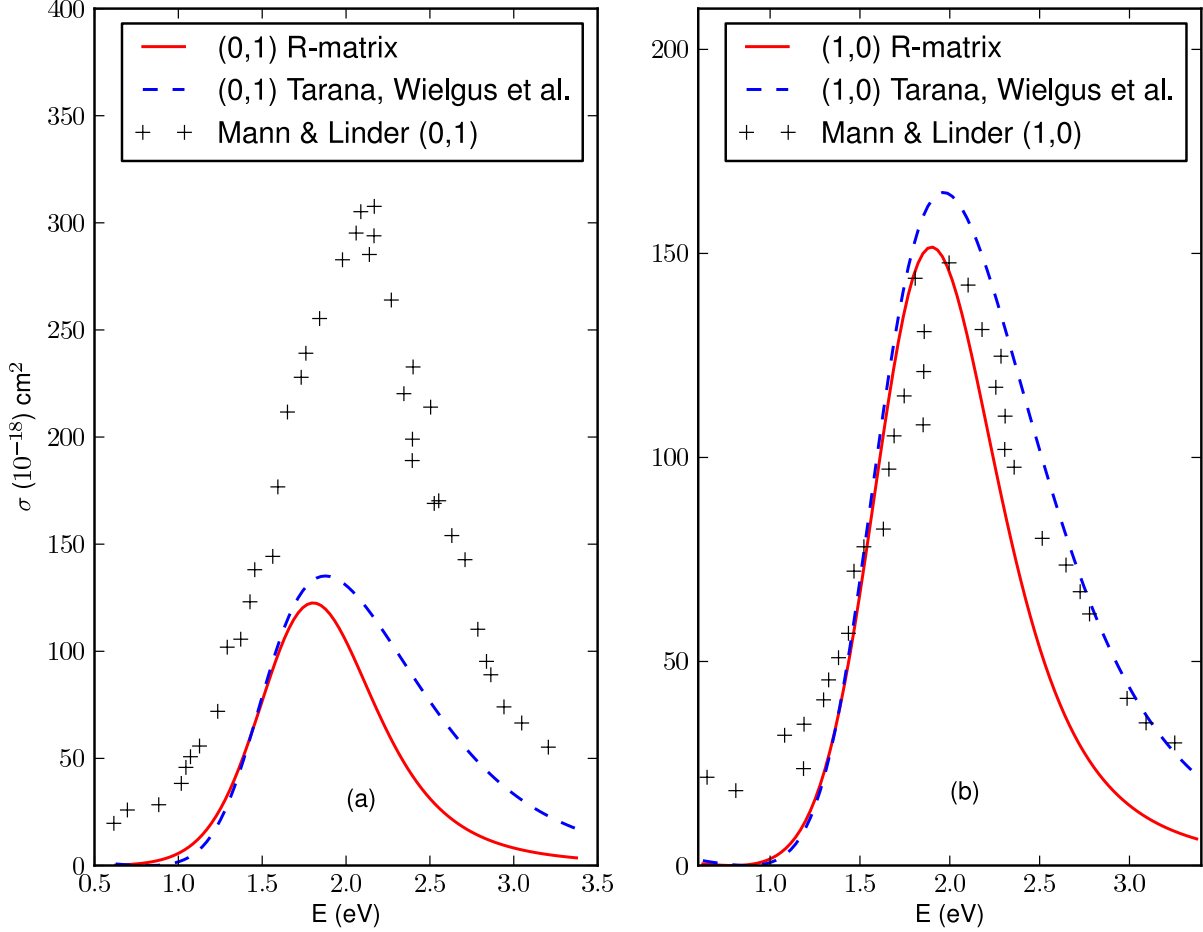


FIG. 6. VE cross sections from the ground vibrational state to the lowest excited state of the C-Cl stretching mode (a) and the lowest excited state of the umbrella mode (b). Results calculated using the *R*-matrix complex PES are compared with cross sections obtained from the previously published model [1] and experimental results due to Mann and Linder [12].

final vibrational state is understandable, since the target vibrational eigenfunctions become spatially more extended with increasing vibrational state (ν_2, ν_3) . This means that the different behavior of corresponding complex PES farther from equilibrium will have larger influence on results, as can be seen in Eq. (4).

V. CONCLUSION

The *ab initio* *R*-matrix method allowed us to calculate the complex two-dimensional PES for CF_3Cl collisions. We used then DVR method to obtain the solution of coupled

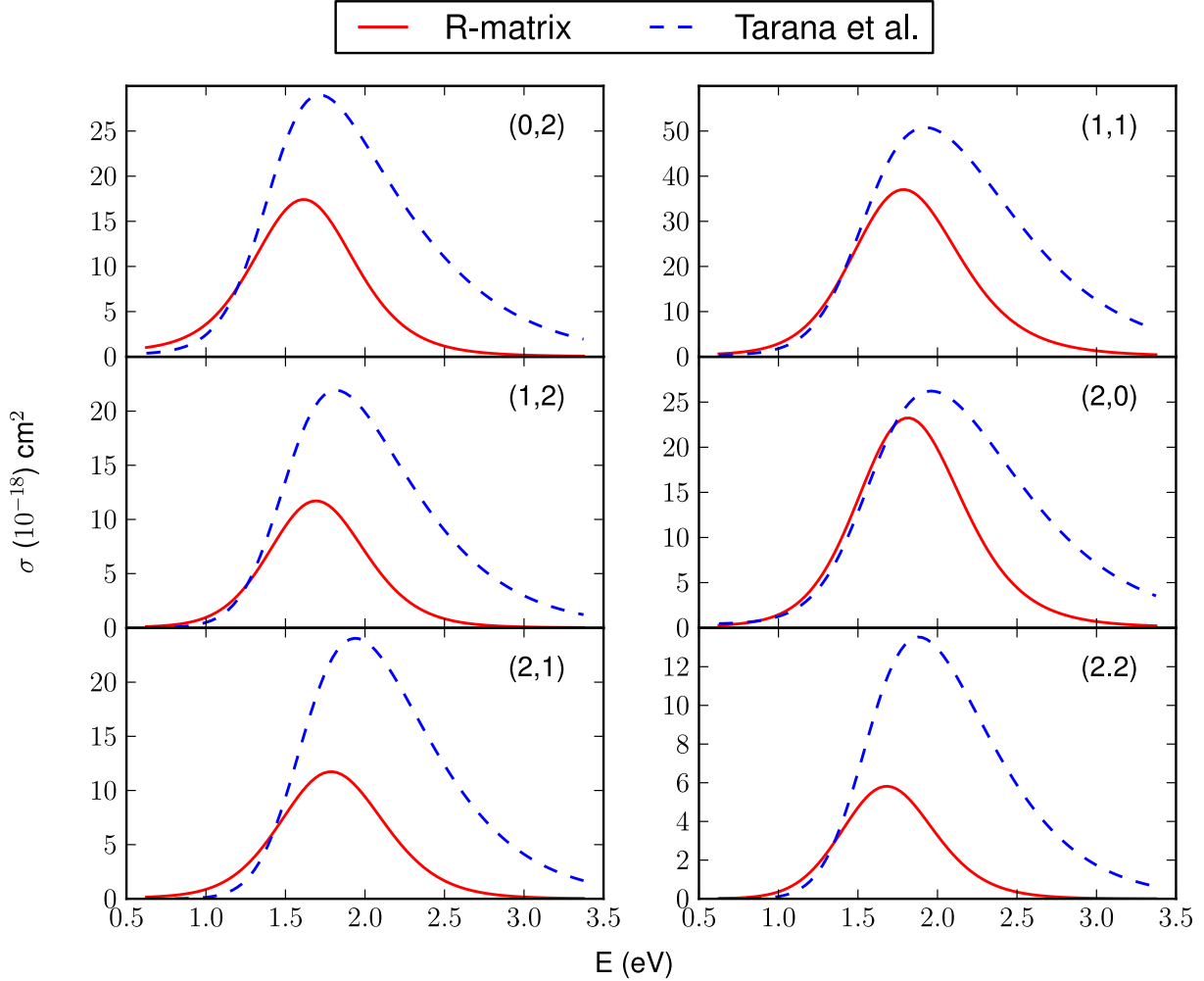


FIG. 7. VE cross sections for excitation from the target vibrational ground state to higher excited states. Results obtained from the complex PES constructed from the *R*-matrix results (solid line) are compared with cross sections calculated using the PES described in [1] (dashed line).

stationary equations (4), and DEA and VE cross sections for the e -CF₃Cl collision process. Our results for the total DEA cross section and the cross section for VE of the umbrella mode agree quite well with experiments, In addition we obtained the final-state vibrational distribution in the CF₃ fragment free of instabilities found in our previous calculations. However our cross sections for VE of the C-Cl stretching mode are significantly lower than the experimental results of Mann and Linder [12] and the results of previous semiempirical one-dimensional calculations [13]. This is something one might expect because of the extra inelastic channels of excitation of umbrella mode that leads to a redistribution of the flux. However, disagreement of the present 2-dimensional results with the experiment is puzzling

478 and requires a further investigation.

479 ACKNOWLEDGMENTS

480 This work was supported in part by the Department of Energy, Office of Science, the
481 National Science Foundation under Grants No. PHY-0652866, No. PHY-0969381, and by a
482 Marie Curie International Incoming Fellowship (FP7-PEOPLE-2009-IIF-252714). Support
483 from the Czech Science Foundation (GAČR) by Grant No. 208/10/1281 and by Záměr
484 MSM0021620860 of the Ministry of Education, Youth and Sports of the Czech Republic is
485 also gratefully acknowledged.

-
- 486 [1] M. Tarana, P. Wielgus, S. Roszak, and I. I. Fabrikant, Phys. Rev. A, **79**, 052712 (2009).
487 [2] A. Kazansky, J. Phys. B: At. Mol. Opt. Phys., **28**, 3987 (1995).
488 [3] D. J. Haxton, Z. Zhang, H.-D. Meyer, T. N. Rescigno, and C. W. McCurdy, Phys. Rev. A,
489 **69**, 062714 (2004).
490 [4] S. T. Chourou and A. E. Orel, Phys. Rev. A, **77**, 042709 (2008).
491 [5] S. T. Chourou and A. E. Orel, Phys. Rev. A, **80**, 032709 (2009).
492 [6] S. T. Chourou and A. E. Orel, Phys. Rev. A, **80**, 034701 (2009).
493 [7] C. W. McCurdy and J. L. Turner, J. Chem. Phys., **78**, 6773 (1983).
494 [8] T. N. Rescigno, W. A. Isaacs, A. E. Orel, H.-D. Meyer, and C. W. McCurdy, Phys. Rev. A
495 **65**, 032716 (2002).
496 [9] D. J. Haxton, Z. Zhang, H.-D. Meyer, T. N. Rescigno, and C. W. McCurdy, Phys. Rev. A
497 **69**, 062714 (2004).
498 [10] H.-D. Meyer, U. Manthe, and L. S. Cederbaum, Chem. Phys. Lett. **165**, 73 (1990).
499 [11] M. H. Beck, A. Jäckle, G. A. Worth, and H.-D. Meyer, Phys. Rep. **324**, 1 (2000).
500 [12] A. Mann and F. Linder, J. Phys. B: At. Mol. Opt. Phys., **25**, 1621 (1992).
501 [13] R. S. Wilde, G. A. Gallup, I. I. Fabrikant, J. Phys. B: At. Mol. Opt. Phys., **32**, 663 (1999).
502 [14] A. M. Lane and R. G. Thomas, Rev. Mod. Phys., **30**, 257 (1958).
503 [15] J. Tennyson, Phys. Rep., **491**, 29 (2010).
504 [16] T. N. Rescigno and C. W. McCurdy, Phys. Rev. A, **62**, 032706 (2000).

- [17] K. Houfek, T. N. Rescigno, and C. W. McCurdy, Phys. Rev. A, **77**, 012710 (2008).
- [18] A. D. McLean and G. S. Chandler, J. Chem. Phys., **72**, 5639 (1980).
- [19] R. Krishnan, J. S. Binkley, R. Seeger, and J. A. Pople, J. Chem. Phys., **72**, 650 (1980).
- [20] J. Juracy R. Lucena, E. Ventura, S. A. do Monte, R. C. M. U. Araújo, M. N. Ramos, and R. Fausto, J. Chem. Phys., **127**, 164320 (2007).
- [21] J. Ying, C. Mathers, K. Leung, H. Pritchard, C. Winstead, and V. McKoy, Chem. Phys. Lett., **212**, 289 (1993).
- [22] D. R. Lide, *CRC Handbook of Chemistry and Physics, 88th Edition (Crc Handbook of Chemistry and Physics)* (CRC, 2007) ISBN 0849304881.
- [23] K. Scanlon, I. Suzuki, and J. Overend, J. Chem. Phys., **74**, 3735 (1981).
- [24] M. Suto and N. Washida, J. Chem. Phys., **78**, 1012 (1983).
- [25] K. Aflatooni and P. D. Burrow, Int. J. Mass Spectrom., **205**, 149 (2001).
- [26] R. F. Frey and J. Simons, J. Chem. Phys., **84**, 4462 (1986).
- [27] T. H. J. Dunning, J. Chem. Phys. **90**, 1007 (1989).
- [28] A. Faure, J. D. Gorfinkiel, L. A. Morgan, and J. Tennyson, Computer Physics Communications **144**, 224 (2002).
- [29] T. Beyer, B. M. Nestmann, and S. D. Peyerimhoff, Chemical Physics, **255**, 1 (2000).
- [30] T. Underwood-Lemons, D. C. Winkler, J. A. Tossell, and J. H. Moore, J. Chem. Phys., **100**, 9117 (1994).
- [31] T. J. Gil, B. H. Lengsfeld, C. W. McCurdy, and T. N. Rescigno, Phys. Rev. A, **49**, 2551 (1994).
- [32] M. H. Mittleman and R. E. von Holdt, Phys. Rev., **140**, A726 (1965).
- [33] I. I. Fabrikant, Sov. Phys. JETP, **44**, 77 (1976).
- [34] R. K. Jones, J. Chem. Phys., **84**, 813 (1986).
- [35] O. H. Crawford, The Journal of Chemical Physics, **47**, 1100 (1967).
- [36] G. A. Gallup and I. I. Fabrikant, Phys. Rev. A, **75**, 032719 (2007).
- [37] T. Underwood-Lemons, T. J. Gergel, and J. H. Moore, J. Chem. Phys., **102**, 119 (1995).
- [38] I. I. Fabrikant, J. Phys.: Conf. Ser. **192**, 012002 (2009).